

# Chip-Based Microwave-Photonic Radar for High-Resolution Imaging

Simin Li, Zhengze Cui, Xingwei Ye, Jing Feng, Yue Yang, Zhengqiang He, Rong Cong, Dan Zhu, Fangzheng Zhang, and Shilong Pan\*

Radar is the only sensor that can realize target imaging at all time and all weather, which would be a key technical enabler for future intelligent society. Poor resolution and large size are the two critical issues for radar to gain ground in civil applications. Conventional electronic radars are difficult to address due to both issues, especially in the Ka band or lower. In this work, a chip-based microwave-photonic radar based on silicon photonic platform, which can implement high-resolution imaging with very small footprint, is proposed and experimentally demonstrated. Both the wideband signal generator and the de-chirp receiver are integrated on the chip. A broadband microwave-photonic imaging radar occupying the full Ku band is experimentally established. A high-precision range measurement with a resolution of 2.7 cm and an error of less than 2.75 mm is obtained. Inverse synthetic aperture imaging of multiple targets with complex profiles is also implemented.

## 1. Introduction

With the unique capability of target imaging at all time and all weather, imaging radar will play an increasingly important role for future intelligent society.<sup>[1]</sup> Chip-based imaging radars are critical for miniaturized platforms such as unmanned aerial vehicles (UAVs), autonomous vehicles, or even mobile devices to navigate and sense the environment due to the great benefits on the reductions of cost, power consumption, volume, and weight. With the fast development of the monolithic microwave integrated circuit (MMIC) technology, a number of chip-based radars have been demonstrated.<sup>[2–6]</sup> For radar imaging, a waveform with a large bandwidth is usually required to achieve a high resolution because the range resolution is inversely proportional to the bandwidth. However, it is challenging for electronic chip-based radars to generate and process broadband waveforms especially in the Ka band or lower. For instance, Wang et al. reported a

Ku-band on-chip radar transceiver with a recorded bandwidth of 1.48 GHz for UAV application, corresponding to a range resolution of about 11.2 cm that is insufficient for the detection of small targets.<sup>[6]</sup>


On the other hand, photonic signal generation and processing provides distinct features in terms of wide frequency coverage, broad instantaneous bandwidth, low frequency-dependent loss, and immunity to electromagnetic interference, which could be a key technical enabler for future ultrahigh resolution and real-time imaging radar. In 2014, Ghelfi et al. proposed a photonics-based coherent radar by employing a mode-locked laser (MLL) to realize both signal generation and sampling.<sup>[7]</sup> After that, different photonic radar architectures

have been demonstrated. In the transmitter, large bandwidth linear frequency-modulated (LFM) signals were generated by optical frequency multiplication,<sup>[8–10]</sup> optical heterodyning,<sup>[11]</sup> or photonic digital-to-analog converter.<sup>[12]</sup> In the receiver, the echoes were handled by photonic time-stretched processing,<sup>[8,11]</sup> photonic de-chirping,<sup>[9,12]</sup> or photonic balanced I/Q de-chirping.<sup>[13]</sup> Ultrahigh resolution radar imaging up to 1.3 cm was reported.<sup>[14]</sup> Application scenarios of the microwave-photonic radars have also been investigated, such as aircraft/UAV/maritime traffic detection,<sup>[7,8,15,16]</sup> automotive sensing,<sup>[17]</sup> and landslides monitoring.<sup>[18]</sup>

Although the existing achievements have demonstrated a significantly improved performance and showed a great potential of the photonic radar, all of the reported microwave-photonic radars are constructed based on discrete optical components, leading to a bulky system with low reliability. Thanks to the long-standing efforts devoted to the photonic integration technologies, chip-based microwave-photonic radar with a dramatic reduction in the footprint is becoming possible.<sup>[19]</sup> Many integrated microwave photonic subsystems were reported previously, including microwave photonic filter,<sup>[20]</sup> microwave photonic true time delay line,<sup>[21]</sup> optical beamformer,<sup>[22]</sup> optoelectronic oscillator,<sup>[23]</sup> programmable photonic signal processor,<sup>[24]</sup> and so on.

In this article, we demonstrate a chip-based microwave-photonic imaging radar based on silicon photonic platform. Both the photonic frequency-doubled LFM signal generator and the photonic de-chirp receiver are integrated on a chip with a footprint of 1.45 mm × 2.5 mm. In a proof-of-concept experiment, a microwave-photonic radar with a bandwidth covering

Dr. S. Li, Z. Cui, X. Ye, J. Feng, Y. Yang, Z. He, R. Cong, Prof. D. Zhu, Prof. F. Zhang, Prof. S. Pan  
Key Laboratory of Radar Imaging and Microwave Photonics  
Ministry of Education  
Nanjing University of Aeronautics and Astronautics  
Nanjing 210016, China  
E-mail: pans@nuaa.edu.cn

 The ORCID identification number(s) for the author(s) of this article can be found under <https://doi.org/10.1002/lpor.201900239>

DOI: 10.1002/lpor.201900239

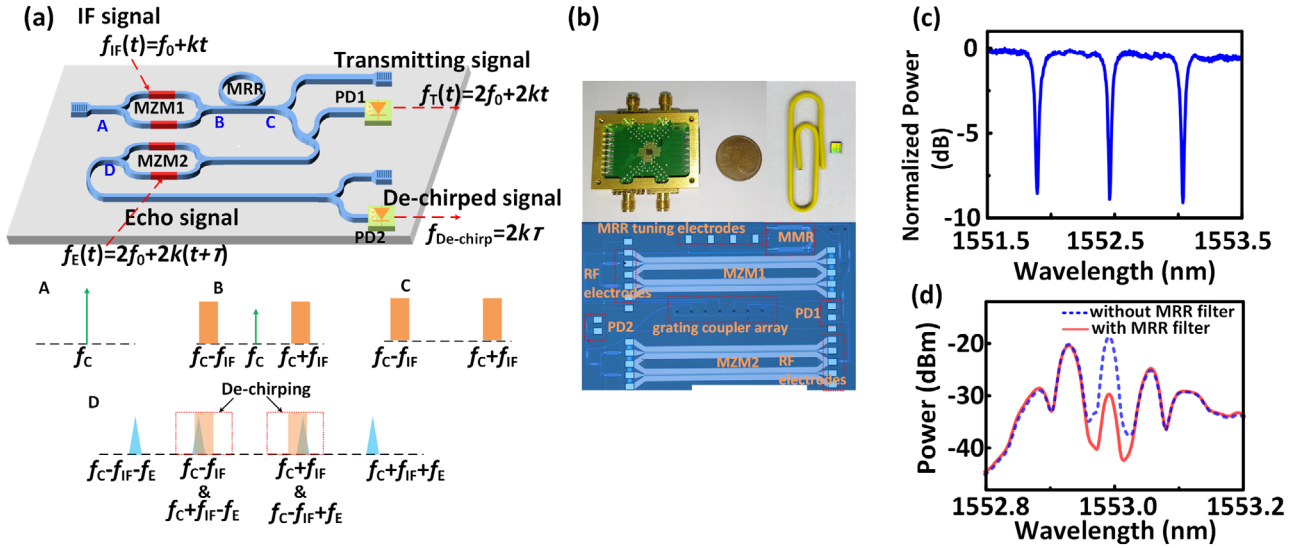


**Figure 1.** a) Schematic diagram of the proposed chip-based microwave-photonic radar. b) The picture and zoom-in view of the fabricated chip. c) Transmission response of the micro-ring resonator (MRR). d) The spectra of the optical double sideband suppressed-carrier modulation (DSB-SC) signal without (blue dash line) and with (red solid line) the incorporation of the MRR filter.

the full Ku-band (12–18 GHz) is established. A high-precision distance measurement with an error of less than 2.75 mm is implemented, and inverse synthetic aperture radar (ISAR) imaging with a resolution of 2.7 cm is achieved.

## 2. Principle and Experiment Results

Figure 1a shows the schematic of the chip-based microwave-photonic radar. An optical carrier with a frequency of  $f_c$  from a tunable laser source is coupled into the chip via a grating coupler, which is then sent into an on-chip Mach-Zehnder modulator (MZM1). MZM1 is driven by an intermediate-frequency (IF) LFM signal with an expression of  $f_{IF}(t) = f_0 + kt$ , where  $f_0$  and  $k$  are the initial frequency and chirp rate, and is biased at the lowest transmission point to suppress the optical carrier. A micro-ring resonator (MRR) filter is followed to enhance the carrier suppression. Ideally, only the  $\pm$  first-order sidebands with frequencies of  $f_{MZM1}(t) = f_c \pm (f_0 + kt)$  would be output from the MRR. Then the optical signal is separated into two paths by a 3-dB optical coupler. In the upper path, the optical signal is sent to a photodetector (PD1) to generate the frequency-doubled LFM signal, of which the frequency is expressed by  $f_T(t) = 2f_0 + 2kt$ . The frequency-doubled signal is amplified by an electrical amplifier and emitted through an antenna to the free space. In the lower path, the optical signal is employed as the local signal for de-chirp processing of the received signal. The received signal is amplified by a low noise amplifier (LNA) and sent to the radio frequency (RF) port of a second MZM (MZM2). For the simplest scenario with a point target, the echo signal is a replica of the transmitting signal with a time delay of  $\tau$  that can be written as  $f_E(t) = 2f_0 + 2k(t + \tau)$ . The optical signal output from MZM2 includes two optical carriers with frequencies of  $f_{MZM1}(t) = f_c \pm (f_0 + kt)$ , and their respective  $\pm$  first-order sidebands with frequencies of  $f_{MZM2(+)}(t) = f_c + (f_0 + kt) \pm (2f_0 + 2kt + 2k\tau)$  and  $f_{MZM2(-)}(t) = f_c -$

$(f_0 + kt) \pm (2f_0 + 2kt + 2k\tau)$ . Then, it is sent to another PD (PD2) to obtain the de-chirped signal with a low frequency of  $f_{de-chirp}(t) = 2k\tau$ . As a result, the distance of the target can be calculated by<sup>[9]</sup>

$$L = \frac{cT}{2B} f_{de-chirp} \quad (1)$$

where  $c$  is the velocity of light,  $T$  and  $B$  are the pulse width and bandwidth of the generated LFM signal, respectively. Due to the fact that low-frequency de-chirped signal can be processed by a low-speed analog-to-digital converter (ADC), real-time ISAR imaging for moving targets can be easily achieved. The range resolution of the radar is determined by the 3-dB bandwidth of the de-chirped signal  $\Delta f_{3dB}$ , i.e.,

$$L_{RES} = \frac{cT}{2B} \Delta f_{3dB} \quad (2)$$

For an ideal case,  $\Delta f_{3dB} = 1/T$ , so the best resolution that can be achieved is  $L_{RES} = c/2B$ .

The proposed chip is fabricated in imec's silicon photonics platform (iSIPP50G). Figure 1b shows the images of the chip captured by a camera and a microscope. The footprint of the chip-based photonic radar is about 1.45 mm  $\times$  2.5 mm. The MRR is designed as the racetrack shape with a perimeter of 996.6  $\mu$ m. Figure 1c shows the measured transmission response of the MRR, which has a free-spectral range (FSR) of 0.57 nm and an extinction ratio of 9 dB. The MZMs and PDs are extracted from the device library of iSIPP50G. In order to monitor the optical spectral response, some optical output ports are introduced. The light is coupled into and out of the chip using a fiber array through a grating coupler array with an interval of 127  $\mu$ m. The measured fiber to fiber insertion loss is about 10 dB.

To investigate the performance of the chip-based microwave-photonic radar, an experiment is carried out. A continuous-wave

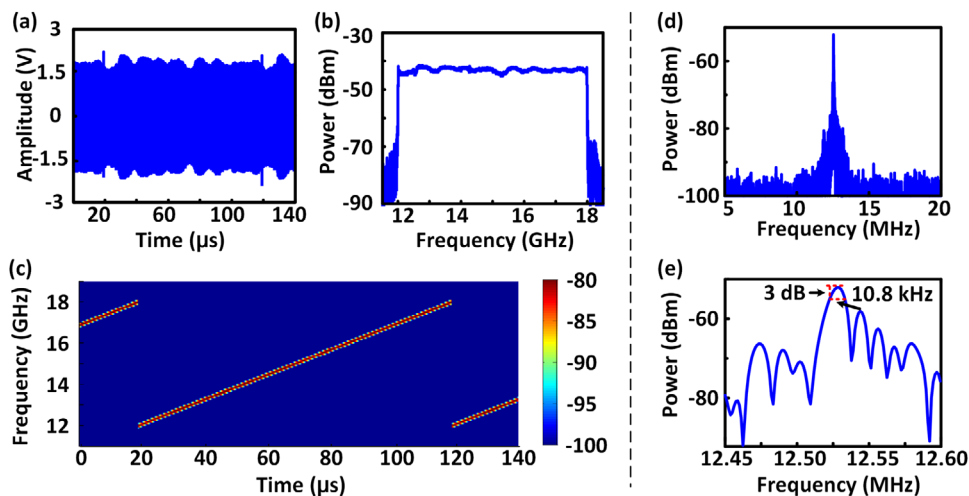


**Figure 2.** The measured results of the generated frequency-doubled linear frequency-modulated signal and the de-chirped signal. a) The time-domain waveform, b) the electrical spectrum, and c) the instantaneous frequency of transmitting signal. d) The electrical spectrum and e) the zoom-in view around the main peak of de-chirped signal.

(CW) light with a wavelength of 1552.9 nm is coupled into the chip via a polarization controller. An arbitrary waveform generator (Tektronix AWG70000) produces an IF-LFM signal with a bandwidth of 3 GHz (6–9 GHz) and a pulse width of 100  $\mu\text{s}$ . The IF-LFM signal and a direct current (DC) bias signal are combined by a bias-tee and then fed into a microwave probe which is connected to the RF electrodes of MZM1. By adjusting the DC bias and tuning the MRR's resonator wavelength to align the optical carrier, a double-sideband modulated optical signal with the carrier suppressed is obtained. Figure 1d illustrates the spectra of the double sideband suppressed-carrier (DSB-SC) modulation signal without and with the incorporation of the MRR filter. The best carrier suppression state for the on-chip MZM by adjusting the DC bias still exhibits a strong optical carrier, shown as the blue dashed line in Figure 1d. A possible reason is that a phase difference between the two arms of the MZM is introduced by the free-carrier dispersion and the thermo effects, leading to an unideal DSB-SC modulation. When the resonator wavelength of the MRR is tuned to filter the optical carrier, the optical carrier is more than 5 dB lower than the sideband according to the red solid line in Figure 1d.

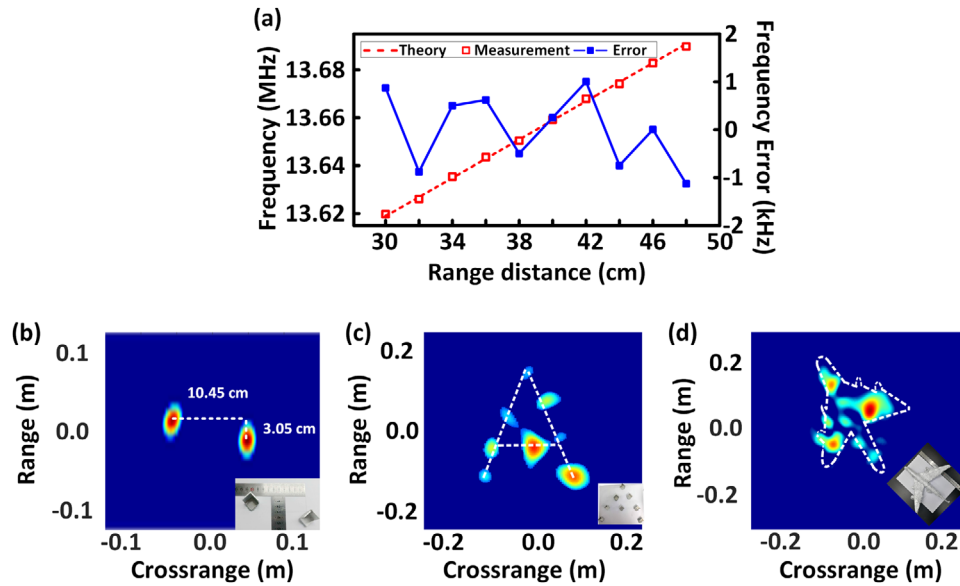
The optical DSB-SC signal is then coupled out of the chip and sent into a PD to perform the optical-to-electrical conversion. Amplified by a low-noise amplifier (LNA) and filtered by an electrical band-pass filter, the frequency-doubled LFM signal is emitted to the free space by a horn antenna. The echo signal collected by a second horn antenna is amplified by another LNA and then launched to drive MZM2 on the chip. The output optical signal is detected by another PD, and the generated electrical signal is sampled by a real-time oscilloscope (Keysight 93304).

Figure 2 shows the experimental results of the generated frequency-doubled LFM signal and the de-chirped signal. The generated frequency-doubled LFM transmitting signal is captured by the real-time oscilloscope with a sampling rate of 80 GSa  $\text{s}^{-1}$  as shown in Figure 2a. The spectrum and time-frequency relationship are calculated using fast Fourier transform (Figure 2b) and short-time Fourier transform (Fig-

ure 2c), respectively. As can be seen, the transmitting signal covers the full Ku-band (12–18 GHz) with a bandwidth of 6 GHz. The pulse width is 100  $\mu\text{s}$ . The power variation of the signal is within  $\pm 1$  dB and the out-of-band spurious rejection ratio is greater than 25 dB. The power ripple is comparable to that of the on-chip electronic radar.<sup>[6]</sup> It should be noted that frequency multiplication with a higher multiplication factor is also possible if the modulation index is increased, the DC bias is properly set and the wavelength of the MRR is carefully adjusted.<sup>[25]</sup>

To evaluate the wideband de-chirp processing capability of the chip, the generated frequency-doubled LFM signal is modulated on MZM2 directly without emitting to the free space by the transmit antenna. The de-chirped signal is sampled by the real-time oscilloscope with a sampling rate of 100 MSa  $\text{s}^{-1}$ . Figure 2d,e shows the spectra performed by the fast Fourier transform of the captured data with a time window of 100  $\mu\text{s}$ . A low-frequency component at 12.5 MHz with a 3 dB bandwidth of 10.8 kHz is achieved. According to Equation (2), the range resolution is about 2.7 cm, which is very close to the theoretical value of 2.5 cm determined by the signal bandwidth.<sup>[9]</sup> It should be noted that there is a sidelobe with a sidelobe suppression ratio of  $\approx 6$  dB, 15.5 kHz apart from the main peak. This sidelobe should be caused by the RF crosstalk between the probes connected to the two MZMs on the chip, which could be suppressed by carefully designing the RF packaging.

A measurement of the target with a varying distance to the antennas is implemented to evaluate the range measurement accuracy. The target is placed about 30 cm away from the antennas initially and then the distance is increased to 46 cm with a step of 2 cm. Figure 3a shows the measured results. The measured frequency errors are kept within  $\pm 1.1$  kHz, corresponding to a range error of less than 2.75 mm. Then, the ISAR imaging experiment is implemented. The targets to be detected are placed on a turntable with a speed of about 360° per second. The de-chirped signal is sampled by the real-time oscilloscope with a sampling rate of 50 MSa  $\text{s}^{-1}$ . The ISAR images are constructed based on 2D Fourier transformation. First, two targets are placed on the



**Figure 3.** a) The measured frequency of the de-chirped signal for a target moved from 30 to 46 cm with a step of 2 cm. ISAR images of b) two targets, c) multiple targets, and d) an airplane model.

turntable with range and cross-range distances of 3 and 10 cm, respectively. Figure 3b shows the obtained ISAR image. The two targets can be clearly distinguished, with the range and cross-range distances of 3.05 and 10.45 cm that agree well with the actual value. The image of multiple targets like a capital “A” constitute by eight trihedral corner reflectors is shown in Figure 3c, which also confirms the high resolution of the chip-based microwave-photonic radar. Finally, the ISAR image of an airplane model with a 28 cm body and a 32 cm wingspan is also obtained, as shown in Figure 3d.

### 3. Discussion

As can be seen in Figure 1b, compared with the microwave-photonic radar constructed by discrete devices, the chip has reduced the volume by hundreds of times, which will also dramatically lower the power consumption and cost, as well as increase the reliability. Although silicon photonics is the most promising solution for photonic integration technology for optical digital systems such as optical communication and data center, its application for microwave technology was not seen as having a bright future in the past, which are mainly due to the limited linearity of the silicon carrier-depletion MZM and the high insertion loss of the optical components. The successful demonstration of on-chip microwave-photonic radar in this work not only proposes a feasible architecture but also shows that the devices developed in silicon photonics can generate a broadband analog waveform with perfect spectral flatness and spur suppression ratio, perform analog mixing for de-chirp processing of broadband LFM signal, and maintain sufficient stability and phase coherence for radar imaging with high resolution. In fact, the linearity of the MZM is not important for the radar transmitter because the input IF LFM signal has a constant profile. For the receiver, the linearity of the MZM is also sufficient for broadband radar imaging, because the LFM signal itself would provide a large gain from

pulse compression. In this work, the optically generated LFM signal has a bandwidth of 6 GHz and a duration of 100  $\mu$ s, leading to a pulse compression gain of 57.8 dB. Considering that the spurious-free dynamic range of the silicon MZM can now reach 110 dB  $\text{Hz}^{2/3}$ ,<sup>[26]</sup> the equivalent dynamic range of the chip-based microwave-photonic radar would approach 103 dB, which is favorable as compared to the electronic on-chip radars.

The power budget among different components should be carefully considered to ensure an acceptable sensitivity for radar detection, as there is no mature optical amplifier in silicon photonics in the current stage. The loss of our chip includes the coupling loss of  $\approx 5$  dB for the grating coupler,  $\approx 9$  dB insertion loss for each MZM, and about 1.5 dB loss for the MRR. In addition, three  $1 \times 2$  power splitters are inserted to monitor the performance of the MZMs and the MRR, which introduced more than 9 dB additional loss. To compensate the loss, a high-power input light and high-gain LNAs are used in the experiment. However, recent works have reduce the insertion loss of the silicon MZM to 3.5 dB<sup>[27]</sup> and the grating loss to 0.9 dB.<sup>[28]</sup> The splitters that are used to monitor the devices can be designed to have an unequal splitting ratio. Therefore, the total loss would be comparable to the systems based on discrete components. In addition, hybrid III–V-on-silicon semiconductor optical amplifier was reported,<sup>[29]</sup> which may be incorporated in the system to boost the optical power.

As the first version of chip-based microwave-photonic radar, we have to say, our implementation does not give full play to the advantages of photonics since only the simplest structure of the chip-based microwave photonic radar is demonstrated. In the future, advanced configuration of the silicon MZMs may be applied to achieve higher frequency multiplication factor.<sup>[9]</sup> The main difference between the electrical and optical frequency multiplications is that the optical method has an intermediate state in the optical domain, so we can remove most of the undesirable frequency components by applying wideband coherent cancellation

or using an optical filter. A large-bandwidth and high-frequency waveform with low spur level can be, thus, generated.

Photonic I/Q mixing or image-reject mixing for wideband de-chirping is another aspect to improve the performance of the chip-based microwave-photonic radar.<sup>[30,31]</sup> Frequency mixing always generates a large number of undesired frequency components and is easily interfered by the signals or noise at the image frequencies. Electronic approaches apply filters to remove some of the mixing spurs and out of band noise, which, however, restricts the instantaneous bandwidth of the system. Photonic I/Q mixing or image-reject mixing can apply wideband coherent cancellation to overcome this problem using optical 90° hybrid or microwave photonic phase shifters,<sup>[30,31]</sup> which not only ensures a wideband de-chirping, but also eliminates the frequency mixing between radar echoes of different targets.<sup>[13]</sup>

Wavelength-division multiplexing may also be adopted for the chip-based system, which opens the possibility for on-chip arrayed radar or MIMO radar with reduced hardware resources.

Up to now, the bandwidth of a silicon MZM can reach 60 GHz,<sup>[32]</sup> and a CMOS-compatible germanium photodiodes with a bandwidth of 67 GHz was reported.<sup>[33]</sup> Therefore, a chip-based microwave-photonic radar with a frequency up to U band (60 GHz) can be possibly implemented. The large bandwidth would enable a reconfigurable or multifunction on-chip microwave photonic radar.

In addition, since the fabrication of the chip is CMOS-compatible, it is feasible to integrate both the photonic circuits and the electrical components on the same chip, leading to a fully integrated microwave-photonic radar with high resolution for miniaturized platforms such as UAVs and autonomous vehicles.

## 4. Conclusion

In conclusion, we have proposed and experimentally demonstrated a chip-based microwave-photonic radar based on the silicon photonic platform. Key optical devices in the radar transceiver are integrated on a single chip, which can generate the frequency-multiplied LFM signal and perform the wideband de-chirp processing required for high-resolution radar imaging. A chip-based microwave-photonic radar covering the full Ku band is established, which realizes a range resolution of 2.7 cm and a measurement error of less than 2.75 mm. High-resolution ISAR imaging of two and multiple targets and a complex-profile object is successfully implemented.

## Acknowledgements

This work was supported in part by the National Key R&D Program of China (2018YFB2201803) and National Natural Science Foundation of China (61527820).

## Conflict of Interest

The authors declare no conflict of interest.

## Keywords

chip-based radar, imaging radar, integrated microwave photonics, microwave-photonic radar, silicon photonics

Received: July 22, 2019

Revised: June 8, 2020

Published online: August 20, 2020

- [1] V. C. Chen, M. Martorella, *Inverse Synthetic Aperture Radar Imaging: Principles, Algorithms and Applications*, SciTech Publishing, London **2014**.
- [2] J. Yu, F. Zhao, J. Cali, F. Dai, D. Ma, X. Geng, Y. Jin, Y. Yao, X. Jin, J. Irwin, R. Jageger, *IEEE J. Solid-State Circuits* **2014**, *49*, 1905.
- [3] R. Ebelt, A. Hamidian, D. Shmakov, T. Zhang, V. Subramanian, G. Boeck, M. Vossiek, *IEEE Trans. Microwave Theory Tech.* **2014**, *62*, 2193.
- [4] G. Pyo, C. Kim, S. Hong, *IEEE Trans. Microwave Theory Tech.* **2017**, *65*, 945.
- [5] Y. Wang, L. Lou, B. Chen, Y. Zhang, K. Tang, L. Qiu, S. Liu, Y. Zheng, *IEEE Trans. Microwave Theory Tech.* **2017**, *65*, 4385.
- [6] Y. Wang, K. Tang, Y. Zhang, L. Lou, B. Chen, S. Liu, L. Qiu, Y. Zheng, in *2016 IEEE Int. Solid-State Circuits Conf. (ISSCC)* (Ed.: Laura C. Fujino), IEEE, Piscataway, NJ **2016**, p. 240.
- [7] P. Ghelfi, F. Laghezza, F. Scotti, G. Serafino, A. Capria, S. Pinna, D. Onori, C. Porzi, M. Scaffardi, A. Malacarne, V. Vercesi, E. Lazzeri, F. Berizzi, A. Bogoni, *Nature* **2014**, *507*, 341.
- [8] R. Li, W. Li, M. Ding, Z. Wen, Y. Li, L. Zhou, S. Yu, T. Xing, B. Gao, Y. Luan, Y. Zhu, P. Guo, Y. Tian, X. Liang, *Opt. Express* **2017**, *25*, 14334.
- [9] F. Zhang, Q. Guo, Z. Wang, P. Zhou, G. Zhang, J. Sun, S. Pan, *Opt. Express* **2017**, *25*, 16274.
- [10] A. Wang, J. Wo, X. Luo, Y. Wang, W. Cong, P. Du, J. Zhang, B. Zhao, J. Zhang, Y. Zhu, J. Lan, L. Yu, *Opt. Express* **2018**, *26*, 20708.
- [11] S. Zhang, W. Zou, N. Qian, J. Chen, *IEEE Photonics Technol. Lett.* **2018**, *30*, 1028.
- [12] S. Peng, S. Li, X. Xue, X. Xiao, D. Wu, X. Zheng, B. Zhou, *Opt. Express* **2018**, *26*, 1978.
- [13] X. Ye, F. Zhang, Y. Yang, S. Pan, *Photonics Res.* **2019**, *7*, 265.
- [14] Y. Yao, F. Zhang, Y. Zhang, X. Ye, D. Zhu, S. Pan, presented at *Optical Fiber Communication Conf.*, San Diego, CA, March 2018.
- [15] F. Zhang, Q. Guo, Y. Yao, P. Zhou, D. Zhu, S. Pan, *Chin. Opt. Lett.* **2017**, *15*, 112801.
- [16] G. Serafino, F. Scotti, L. Lembo, B. Hussain, C. Porzi, A. Malacarne, S. Maresca, D. Onori, P. Ghelfi, A. Bogoni, *J. Lightwave Technol.* **2019**, *37*, 643.
- [17] G. Serafino, F. Amato, S. Maresca, L. Lembo, P. Ghelfi, A. Bogoni, *IET Radar Sonar Navig.* **2018**, *12*, 1179.
- [18] S. Melo, S. Maresca, S. Pinna, F. Scotti, M. Khosravianian, C. Arismar, F. Giannetti, A. Barman, A. Bogoni, *J. Lightwave Technol.* **2018**, *36*, 2337.
- [19] D. Marpaung, J. Yao, J. Capmany, *Nat. Photonics* **2019**, *13*, 80.
- [20] J. Fandiño, P. Muñoz, D. Doménech, J. Capmany, *Nat. Photonics* **2017**, *11*, 124.
- [21] S. Pan, Z. Tang, M. Huang, S. Li, *IEEE J. Sel. Top. Quantum Electron.* **2020**, *26*, 1.
- [22] M. Burla, D. Marpaung, L. Zhuang, A. Leinse, M. Hoekman, R. Heideman, C. Roeloffzen, *IEEE Photonics Technol. Lett.* **2013**, *25*, 1145.
- [23] W. Zhang, J. Yao, *J. Lightwave Technol.* **2018**, *36*, 4655.
- [24] L. Zhuang, C. Roeloffzen, M. Hoekman, K. Boller, A. Lowery, *Optica* **2015**, *2*, 854.
- [25] S. Pan, J. Yao, *IEEE Trans. Microwave Theory Tech.* **2010**, *58*, 1967.
- [26] J. Ding, S. Shao, L. Zhang, X. Fu, L. Yang, *Opt. Express* **2016**, *24*, 24641

- [27] X. Xiao, H. Xu, X. Li, Z. Li, T. Chu, Y. Yu, J. Yu, *Opt. Express* **2013**, *21*, 4116.
- [28] R. Marchetti, C. Lacava, A. Khokhar, X. Chen, I. Cristiani, D. Richardson, G. Reed, P. Petropoulos, P. Minzioni, *Sci. Rep.* **2017**, *7*, 16670.
- [29] K. Gasse, R. Wang, G. Roelkens, *Opt. Express* **2019**, *27*, 293.
- [30] Z. Tang, Y. Li, J. Yao, S. Pan, *Laser Photonics Rev.* **2020**, *14*, 1800350.
- [31] D. Zhu, S. Pan, *Photonics* **2018**, *5*, 6.
- [32] M. Li, L. Wang, X. Li, X. Xiao, S. Yu, *Photonics Res.* **2018**, *6*, 109.
- [33] D. Zhu, J. Zheng, Y. Qamar, O. Martynov, F. Rezaie, E. Preisler, presented at *IEEE 15th Int. Conf. on Group IV Photonics (GFP)*, Cancun, Mexico, August 2018.